In April 2022, Osaka City University and Osaka Prefecture University marge to Osaka Metropolitan University

AlGaN/GaN/3C-SiC on diamond HEMTs with thick nitride layers prepared by bonding-first process

Ryo Kagawa, Keisuke Kawamura, Yoshiki Sakaida, Sumito Ouchi, Hiroki Uratani, Yasuo Shimizu, Yutaka Ohno, Yasuyoshi Nagai, Jianbo Liang, Naoteru Shigekawa

Citation	Applied Physics Express. 15(4); 041003
Issue Date	2022-03-17
Type	Journal Article
Textversion	Author
Highlights	・ダイヤモンドに接合された窒化ガリウム（GaN）を熱加工し、トランジスタ作製に成功。 ・作製したトランジスタの放熱性の向上、接合による GaN 層の品質担保を実証。 ・高品質な炭化ケイ素（3C-SiC）バッファ層を採用。 ・ダイヤモンド上窒化ガリウムの大面積化が可能になり、社会実装を加速。
Relation	This is the Accepted Manuscript version of an article accepted for publication in Applied Physics Express. IOP Publishing Ltd is not responsible for any errors or omissions in this version of the manuscript or any version derived from it. The Version of Record is available online at https://doi.org/10.35848/1882-0786/ac5ba7.
DOI	10.35848/1882-0786/ac5ba7

Self-Archiving by Author(s)
Placed on: Osaka City University

Kagawa, R., Kawamura, K., Sakaida, Y., Ouchi, S., Uratani, H., Shimizu, Y., Ohno, Y., Nagai, Y., Liang, J., & Shigekawa, N. (2022). AlGaN/GaN/3C-SiC on diamond HEMTs with thick nitride layers prepared by bonding-first process. Applied Physics Express. 15, 041003. https://doi.org/10.35848/1882-0786/ac5ba7

概　要

研究グループは、ダイヤモンドに接合された窒化ガリウムを熱加工し、トランジスタの作製に成功するとともに放熱性の向上を実証しました。

窒化ガリウムを利用したトランジスタは、シリコンに代わる次世代半導体として、携帯電話の基地局などで幅広く使用されているものの、動作時の発熱により性能が大きく制限されており、大型の放熱部材も必要とされていました。

研究グループは、2021 年 9 月に世界で初めて GaN とダイヤモンドの直接接合に成功し、1,000 ℃の熱処理にも耐えることを実証しました。今回の研究では、ダイヤモンドとの直接接合に成功した窒化ガリウムに約 800℃の熱処理を行うことで、放熱性に優れたトランジスタの作製に成功しました。地球上で最も熱伝導率が高く、最も効率的に熱を逃すことができるダイヤモンドを使用しているため、シリコン上でのトランジスタと比べて放熱性が向上していること（図 1)、また、窒化ガリウム層の品質が劣化しないことも明らかとなりました。

本研究成果により、接合後にトランジスタを作製することでダイヤモンド上窒化ガリウムの大面積化が進展し、レーダーやインバータなどの大電力用途にも使用範囲が拡大することが期待されます。

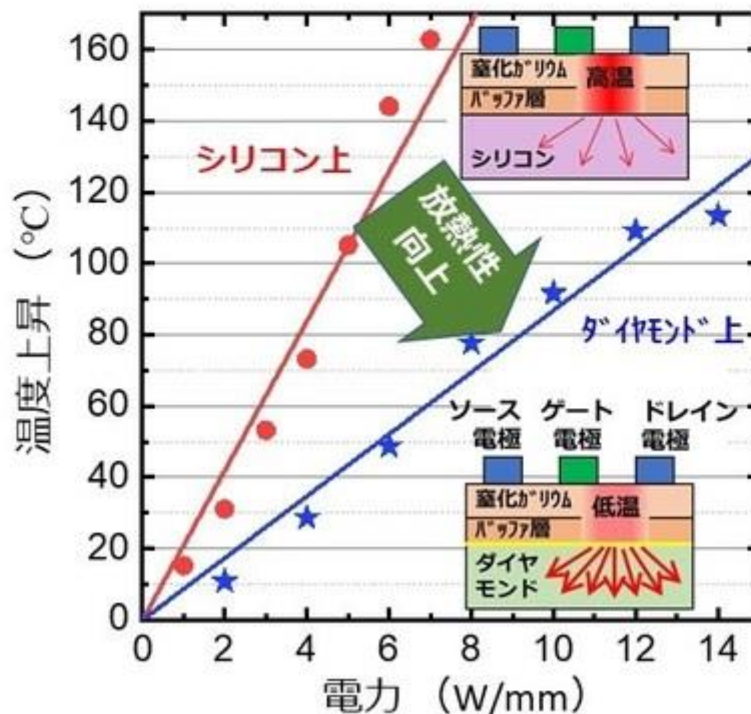

図 1：ダイヤモンド上に作製することによる放熱性の向上効果

（Si 上と比べて放熱性が良いため、同じ電力でも温度上昇は小さい）。

‘ダイヤモンドに接合された窒化ガリウムを熱加工し、トランジスタを作製することに成功’. 大阪市立大学. https://www.osaka-cu.ac.jp/ja/news/2021/220318. (参照　2022-03-18)

AlGaN/GaN/3C-SiC on diamond HEMTs with thick nitride layers prepared by bonding-first process

Ryo Kagawa[1], Keisuke Kawamura[2], Yoshiki Sakaida[2], Sumito Ouchi[2], Hiroki Uratani[2], Yasuo Shimizu[3], Yutaka Ohno[4], Yasuyoshi Nagai[5], Jianbo Liang[1], and Naoteru Shigekawa[1]*

[1] *Department of Electronic Information Systems, Osaka City University, Sugimoto 3-3-138, Sumiyoshi, Osaka 558-8585, Japan*

[2] *The SiC Division, Air Water Inc.2290-1 Takibe, Toyoshina Azumino, Nagano 399-8204, Japan*

[3] *National Institute for Materials Science (NIMS),1-2-1, Sengen, Tsukuba, Ibaraki,305-0047, Japan*

[4] *Institute for Materials Research (IMR), Tohoku University, 2-1-1 Katahira, Sendai 980-8577, Japan*

[5] *Institute for Materials Research (IMR), Tohoku University, 2145-2 Narita, Oarai, Ibaraki 311-1313, Japan*

E-mail: shigekawa@osaka-cu.ac.jp

We fabricate AlGaN/GaN high electron mobility transistors (HEMTs) on diamond substrates by transferring 8-μm heterostructures grown on 3C-SiC/Si templates and subsequently applying the conventional device process steps. No exfoliation of 3C-SiC/diamond bonding interfaces is observed during 800 °C annealing, the essential step for forming ohmic contacts on nitrides. The thermal resistance of HEMTs on diamond is 35% of that of HEMTs on Si, which is assumed to be the origin of smaller negative drain conductance in on-diamond HEMTs. The results imply that the bonding-first process is applicable for fabricating low-thermal-resistance HEMTs with thick nitride layers.

Group-III-nitride based electron devices such as GaN HEMTs have been widely applied for high-power and high-frequency/high-speed systems because of their excellent power capability and electron transport properties. RF power amplifiers made of HEMTs with 1–2-μm-thick nitride layers have become popular in wireless networks [1-2]. Recently, HEMTs made of thicker (>4 μm) nitride layers have been intensively investigated for power circuit applications [3-5]. However, a rise in the temperature of highly biased devices [6-7], which is marked in HEMTs on sapphire substrates because of their low thermal conductivity, causes degradation of device characteristics, such as negative drain conductance (NDC) [8], and brings about negative impacts on their reliability [9]. These self-heating effects have been reduced by using 4H-SiC substrates for nitride growth[6].

To proceed with the improvement of device characteristics, the possibility of using diamond, with thermal conductivity of up to 2,200 W/mK (in the case of single crystalline (SC) diamond), as a heat spreader has been intensively investigated. Nitride heterostructures have been grown on SC diamond (111) substrates [10]. Alternatively, after host substrates for epitaxial growth had been removed, and thin SiN dielectrics and polycrystalline (PC) diamond have been successively deposited on the exposed bottom surfaces [11-12]. Although this technology is applicable to large-size heterostructures, the low thermal conductivities of SiN dielectrics [13] and the PC diamond near bonding interfaces [14] affect the thermal resistance (R_{TH}) of such HEMTs.

To further improve the thermal properties, heterostructures have been transferred onto diamond substrates using wafer bonding technologies such as surface-activated bonding (SAB) [15]. Reported transfer processes include those based on a “device first” concept [16-18], in which heterostructures were bonded to diamonds after HEMTs had been fabricated, and those based on a “bonding first” concept [19], in which HEMTs were fabricated after heterostructures had been transferred. In the device-first process, possible unevenness and/or ununiform strain introduced during device fabrication [20] are assumed to bring about difficulties in bonding large-size samples. Samples have been annealed at 700 °C during bonding in the bonding-first process, which limited the thickness of heterostructures to be bonded (typically < 2 μm) [21]. We have previously fabricated diamond/GaN junctions [22] using SAB without heating and confirmed their tolerance against 1000 °C annealing.

In this work, we transferred AlGaN/GaN heterostructures grown on 3C-SiC/Si (111) templates [23] onto diamond substrates using SAB [24] and subsequently fabricated GaN HEMTs, i.e., the bonding-first process was applied. The total thickness of the nitride layers of the heterostructures is 8 μm. The electrical properties of HEMTs as well as their surface

1 temperature during operation were investigated and compared with those of HEMTs
2 fabricated on as grown heterostructures.

3 We grew an AlGaN/GaN heterostructure consisting of a 23-nm-thick $Al_{0.26}Ga_{0.74}N$ barrier
4 layer, a 6-μm-thick GaN layer, and a 2-μm-thick III-N buffer layer on a (111)-oriented 3C-
5 SiC/Si template by metal organic chemical vapor deposition (CVD). The thickness of the
6 3C-SiC layer was 1 μm. We temporarily bonded the top surface of the heterostructure to a
7 handle Si substrate and removed the host Si substrate with fluonitric acid. Then, we
8 polished the exposed backside of 3C-SiC layer by chemical mechanical polishing. We
9 deposited a ≈10-nm Si layer on a bonding surface of a 10-mm-square, 500-μm-thick single-
10 crystalline CVD-diamond substrate by RF sputtering and fabricated the handle
11 substrate/nitride/3C-SiC/diamond structure using SAB. After the handle Si substrate had
12 been removed with fluonitric acid, we applied the conventional process steps to fabricate the
13 on-diamond HEMTs (Fig. 1): mesa isolation using Ar^+-ion milling, formation of source and
14 drain contacts by evaporating Ti/Al/Ti/Au layers and annealing at 800 °C for 60 s in N_2
15 ambient, and formation of gate contacts by evaporating Ni/Au layers. Top views of the as-
16 bonded handle substrate/nitride/3C-SiC/diamond junction, the junction after removal of the
17 handle substrate, and HEMTs fabricated on diamond are shown in Figs. 2(a)–(c),
18 respectively. A cross-sectional SEM image of HEMTs fabricated on diamond is shown in
19 Fig. 2(d). These images show that a heterostructure with a total thickness of ≈ 9 μm was
20 successfully bonded to diamond and that all process steps, including the 800 °C annealing,
21 were completed without the occurrence of exfoliation at the bonding interfaces. We also
22 applied the same process steps to a heterostructure as grown on the 3C-SiC/Si template (on-
23 Si HEMTs).

24 We investigated the sheet resistance (R_{sh}), contact resistance (R_c), concentration (N_s), and
25 mobility (μ) of two-dimensional electron gas at the AlGaN/GaN interfaces of HEMTs using
26 the transfer length method (TLM) and capacitance-voltage measurement [25] at room
27 temperature. We estimated R_{sh}, R_c, N_s, and μ of the heterostructures on diamond to be 406
28 Ω/sq, 1.6 Ω·mm, 0.86×10^{13} cm^{-2}, and 1780 cm^2/Vs, respectively. Those of the as-grown
29 heterostructures were found to be 398 Ω/sq, 2.3 Ω·mm, 0.89×10^{13} cm^{-2}, and 1760 cm^2/Vs,
30 respectively. The results are summarized in Table I. It is notable that no marked difference
31 in each parameter was observed between the two heterostructures.

32 The drain current (I_D)-drain bias voltage (V_{DS}) characteristics as well as the transfer
33 characteristics of HEMTs with gate length (L_G) of 5 μm, source-to-gate and gate-to-drain
34 separations (L_{SG}, L_{GD}) of 5 μm, and gate width (W_G) of 150 μm were measured for V_{DS}

between 0 and 20 V and gate bias voltage (V_{GS}) varied between -4 and 3 V with a 1-V step. The characteristics of HEMTs on diamond and on Si are shown in Figs. 3(a) and (b), respectively. Excellent pinch-off properties were observed for both devices. In the I_D-V_{DS} curve for V_{GS} = 3 V in the HEMT on Si, we observed a peak in I_D (460 mA/mm) at V_{DS} = 8.9 V and NDC of -7.5 mS/mm for a higher V_{DS} region. The I_D-V_{DS} curve for the same V_{GS} in the HEMT on diamond revealed a peak of 570 mA/mm at V_{DS} = 10.5 V and NDC of -5.6 mS/mm for a higher V_{DS}, i.e., the magnitude of NDC of the on-diamond HEMT was 75% of that of the NDC of the on-Si HEMT, while the peak I_D of the on-diamond HEMT was 1.2 times as large as that of the on-Si HEMT. We also confirmed that threshold voltages of on-diamond and on-Si HEMTs were the same (-3.2 V) and their intrinsic transconductance for V_{GS} lower than -2.5 V agreed with that estimated based on the long-channel model although the epi layer of on-diamond HEMTs experienced the transferring process (not shown).

The temperature of biased TLM devices and HEMTs were measured by using micro-photoluminescence (μ-PL) and micro-Raman (μ-Raman) spectroscopies. During measurements, the dies were mounted on a Cu block. The temperature of its bottom was fixed at 300 K using a water-cooling system. In the μ-PL measurement, a 325-nm He-Cd laser was focused on the surface of the HEMTs. The relationship between the peak energies of PL spectra and ambient temperatures measured for unbiased devices, which was fit to a Varshini equation [26-27], was used as a calibration curve. In the μ-Raman spectroscopy, the Stokes/anti-Stokes ratio measured for the GaN E2(high) band measured using a 488-nm laser was used for estimating temperatures. Results of measurements were compared with those of analysis by the finite element method (FEM), in which we adjusted the thermal conductivity (κ) of the III-N buffer layer to reproduce the measurement results. we referred to k of other materials in the literature [28].

Relationships between the power dissipation (P_{diss}) in 8-μm-long and 220-μm-wide biased TLM devices on diamond and on Si and temperatures at the center of their channels are shown in Fig. 4. The temperature based on the μ-PL measurement was higher than that based on the μ-Raman measurement for the same power dissipation. In this figure, we also show their calculated surface temperature and that averaged along the vertical direction in the GaN channels, which were obtained by setting κ of the III-N buffer layer to 30 W/mK. We found that for each TLM device the calculated surface temperature and the average temperature agreed with the results of the μ-PL and the μ-Raman measurements, respectively. This means that the penetration depths of lights with wavelengths of 325 and 488 nm into GaN, which are ≈ 70 nm and 50 μm [29-30], respectively, cause the higher temperatures observed in the μ-

PL measurements. The results of the analysis imply that the μ-PL measurement is preferable for estimating the temperature of active parts of biased HEMTs and hence their R_{TH}. More importantly, the temperature rise of on-diamond devices was approximately half of that of on-Si devices.

We estimated temperatures in the gap between the source and gate and in the gap between the gate and drain of biased HEMTs with L_G = 20 μm, L_{SG} = L_{GD} = 10 μm, and W_G = 200 μm using μ-PL measurements. V_{DS} was varied for a fixed V_{GS} (2 V) in measurements. The spatial variations of temperatures for on-diamond and on-Si HEMTs for P_{diss} of 2, 4, and 6 W/mm are compared in Fig. 5(a). The highest temperature was observed at the gate edge in the gap between the gate and drain for each bias condition. The relationship between the temperature at this region and P_{diss} is shown in Fig. 5(b). As with the results for TLM devices, lower temperatures were observed for the on-diamond HEMTs in comparison with those for the on-Si HEMTs. R_{TH} of the on-diamond HEMTs [8 K/(W/mm)], was ≈ 35% of that of the on-Si HEMT [26 K/(W/mm)]. In addition, as is shown in Fig. 5(c), relationships between drain current for each P_{diss} normalized by current at 2 W/mm ($I_D(P_{diss})/I_D$(2 W/mm)) and the temperature of gate edge for the two types of HEMTs were close to each other, which implies that the observed lower R_{TH} of the on-diamond HEMTs is assumed to be the origin of their lower NDC. Also notable is that the electrical properties of the on-diamond heterostructures agree with those of the on-Si heterostructures. These features show that the process for transferring heterostructures onto diamond does not have negative impacts on the characteristics of nitride devices fabricated after they have been transferred.

In summary, we transferred 8-μm-thick AlGaN/GaN heterostructures onto CVD-diamond and successfully fabricated HEMTs by applying the conventional device process steps after the transfer. No exfoliation of the heterostructure occurred, although the bonding interface experienced 800 °C annealing to form ohmic contacts. We also observed a smaller R_{TH} in the on-diamond devices (×0.35 of that in on-Si devices), which was assumed to be the origin of 0.75-times smaller NDC of on-diamond HEMTs although its peak I_D was 1.2 times larger than that of on-Si HEMTs. These results imply that the bonding-first approach is applicable for fabricating low-R_{TH} nitride devices and integrated circuits made of thick heterostructures.

Acknowledgment

This research was supported by the Adaptable and Seamless Technology Transfer Program through Target-Driven R&D (A-STEP) from Japan Science and Technology Agency (JST) Grant Number JPMJTM20Q7. The fabrication and SEM observation of the samples were

performed at the Oarai Center and at the Laboratory of Alpha-Ray Emitters in IMR under the Inter-University Cooperative Research in IMR of Tohoku University (202012-IRKMA-0046).

References

1) U. K. Mishra, P. Parikh, and Y. F. Wu, Proceedings of the IEEE **90**, 1022 (2002).
2) N. Keshmiri, D. Wang, B. Agrawal, R. Hou and A. Emadi, IEEE Access **8**, 70553 (2020).
3) K. J. Chen, O. Häberlen, A. Lidow, C. l. Tsai, T. Ueda, Y. Uemoto, and Y. Wu, IEEE Trans. Electron Devices **64**, 779 (2017).
4) B. Rowena, S. L. Selvaraj and T. Egawa, IEEE Electron Device Lett. **32**, 1534 (2011).
5) S. Lawrence Selvaraj, T. Suzue and T. Egawa, IEEE Electron Device Lett. **30**, 587 (2009).
6) M. Kuball, J. M. Hayes, M. J. Uren, T. Martin, J. C. H. Birbeck, R. S. Balmer, and B. T. Hughes, IEEE Electron Device Lett. **23**, 7 (2002).
7) N. Shigekawa, K. Onodera, and K. Shiojima, Jpn. J. Appl.Phys. **42**, 2245 (2003).
8) R. Gaska, A. Osinsky, J. W. Yang, and M. S. Shur, IEEE Electron Device Lett. **19**, 89 (1998).
9) J.W. Pomeroy, M.J. Uren, B. Lambert, M. Kuball, Microelectronics Reliability **55**, 2505 (2015).
10) K. Hirama, M. Kasu, and Y. Taniyasu, "IEEE Electron Device Lett. **33**, 513 (2012).
11) J. W. Pomeroy, M. Bernardoni, D. C. Dumka, D. M. Fanning, and M. Kuball, Appl. Phys. Lett. **104**, 083513 (2014).
12) M. J. Tadjer, T. J. Anderson, M. G. Ancona, P. E. Raad, P. Komarov, T. Y. Bai, J. C. Gallagher, A. D. Koehler, M. S. Goorsky, D. A. Francis, K. D. Hobart, and F. J. Kub, IEEE Electron Device Lett. **40**, 881 (2019).
13) H. Sun, R. B. Simon, J. W. Pomeroy, D. Francis, F. Faili, D. J. Twitchen, and M. Kuball, Appl. Phys. Lett. **106**, 111906 (2015).
14) Y. Zhou, R. Ramaneti, J. Anaya, S. Korneychuk, J. Derluyn, H. Sun, J. Pomeroy, J. Verbeeck, K. Haenen, and M. Kuball, Appl. Phys. Lett. **111**, 041901 (2017).
15) Z. Cheng, F. Mu, L. Yates, T. Suga, and S. Graham, ACS Appl. Mater. Interfaces **12**, 8376 (2020).
16) P. C. Chao, K. Chu, C. Creamer, J. Diaz, T. Yurovchak, M. Shur, R. Kallaher, C. McGray, G. D. Via, and J. D. Blevins, IEEE Trans. Electron Devices **62**, 3658 (2015).
17) K. K. Chu, T. Yurovchak, P. C. Chao and C. T. Creamer, 2013 IEEE CSICS,1 (2013).
18) Y. Minoura, T. Ohki, N. Okamoto, A. Yamada, K. Makiyama, J. Kotani, S. Ozaki, M. Sato, and N. Nakamura, Jpn. J. Appl. Phys. **59**, SGGD03 (2020).
19) M. Trejo, G. H. Jessen, K. D. Chabak, J. K. Gillespie, A. Crespo, M. Kossler, V. Trimble, D. Langley, E. R. Heller, B. Claflin, D. E. Walker, B. Poling, R. Gilbert, G. D. Via, J. Hoelscher, J. Roussos, F. Ejeckam, and J. Zimmer, Phys. Status Solidi A **208**, 439 (2011).
20) O. Nakatsuka, H. Kitada, Y. Kim, Y. Mizushima, T. Nakamura, T. Ohba, and S. Zaima, Jpn. J. Appl. Phys. **50**, 05ED03 (2011).
21) D. Francis, F. Faili, D. Babić, F. Ejeckam, A Nurmikko, H. Maris, Diam. Relat. Mater. **19**, 229 (2010).
22) J. Liang, A. Kobayashi, Y. Shimizu, Y. Ohno, S.-W. Kim, K. Koyama, M. Kasu, Y. Nagai, and N. Shigekawa, Adv. Mater. **33**, 2104564 (2021).
23) A. Bose, D. Biswas, S. Hishiki, S. Ouchi, K. Kitahara, K. Kawamura, and A. Wakejima, IEEE Electron Device Lett. **41**, 1480 (2020).
24) R. Kagawa, K. Kawamura, Y. Sakaida, S. Ouchi, H. Uratani, Y. Shimizu, Y. Ohno, Y. Nagai, N. Shigekawa, and J. Liang, 2021 7th International Workshop on Low Temperature Bonding for 3D Integration (LTB-3D), 15 (2021).
25) O. Ambacher, J. Smart, J. R. Shealy, N. G. Weimann, K. Chu, M. Murphy, W. J. Schaff, L. F. Eastman, R. Dimitrov, L. Wittmer, M. Stutzmann, W. Rieger, and J. Hilsenbeck, J. Appl. Phys. **85**, 3222 (1999).
26) Y.P. Varshni, Physica **34**, 149 (1967).
27) B. Monemar, Phys. Rev. B, **10**, 676 (1974).
28) F. Bertoluzza, N. Delmonte, and R. Menozzi, Microelectron. Reliab. **49**, 468 (2009).
29) L. Lv, X. H. Ma, J. C. Zhang, Z. Bi, L. Y. Liu, H. S. Shan, and Y. Hao, IEEE Trans Nucl Sci. **62**, 300 (2015).
30) Z. C. Feng, M. Schurman, R. A. Stall, M. Pavlosky, and A. Whitley, Appl. Opt. **36**, 2917 (1997).

Figure Captions

Fig. 1. Process steps for fabricating on-diamond HEMTs.

Fig. 2. Top views of (a) as-bonded handle substrate/nitride/3C-SiC/diamond junction, (b) junction after removal of handle substrate, and (c) fabricated on-diamond HEMTs. (d) Cross sectional SEM image of on-diamond HEMTs.

Fig. 3. I_D-V_{DS} characteristics of (a) on-diamond and (b) on-Si HEMTs with L_G = 5 μm, L_{SG} = L_{GD} = 5 μm, and W_G = 150 μm for V_{GS} varied between -4 and 3 V in 1-V steps.

Fig. 4. Relationships between temperature rise and dissipated power density in on-diamond and on-Si TLM devices. Results of measurements based on μ-PL and μ-Raman spectroscopies are compared with those of FEM analysis.

Fig. 5. (a) Spatial variations of temperature on surfaces of on-diamond and on-Si HEMTs for P_{diss} of 2, 4, and 6 W/mm. (b) Relationships between temperature rise at the gate edge in the gate-to-drain separation and P_{diss} for the respective HEMTs. The two lines are eye guides. (c) Relationships between drain current normalized by I_D at P_{diss} of 2 W/mm and the temperature at the gate edge in the gate-to-drain separation for the respective HEMTs.

Table I. Material parameters.

Material parameters	HEMT on Si		HEMT on diamond	
	Average	SD	Average	SD
R_{sh} (Ω/sq)	397	7	406	3
R_c (Ωmm)	2.7	0.1	1.6	0.1
N_s (10^{13}/cm^2)	0.89	0.06	0.86	0.02
μ (cm^2/Vs)	1760	20	1780	30

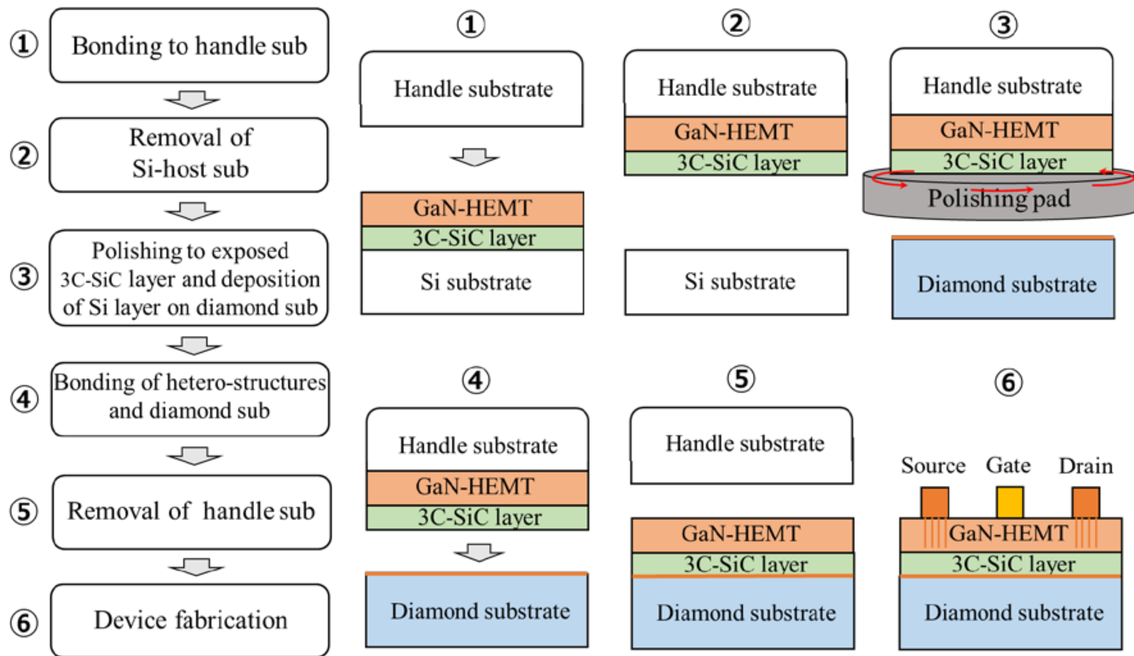

Fig. 1. Process steps for fabricating on-diamond HEMTs.

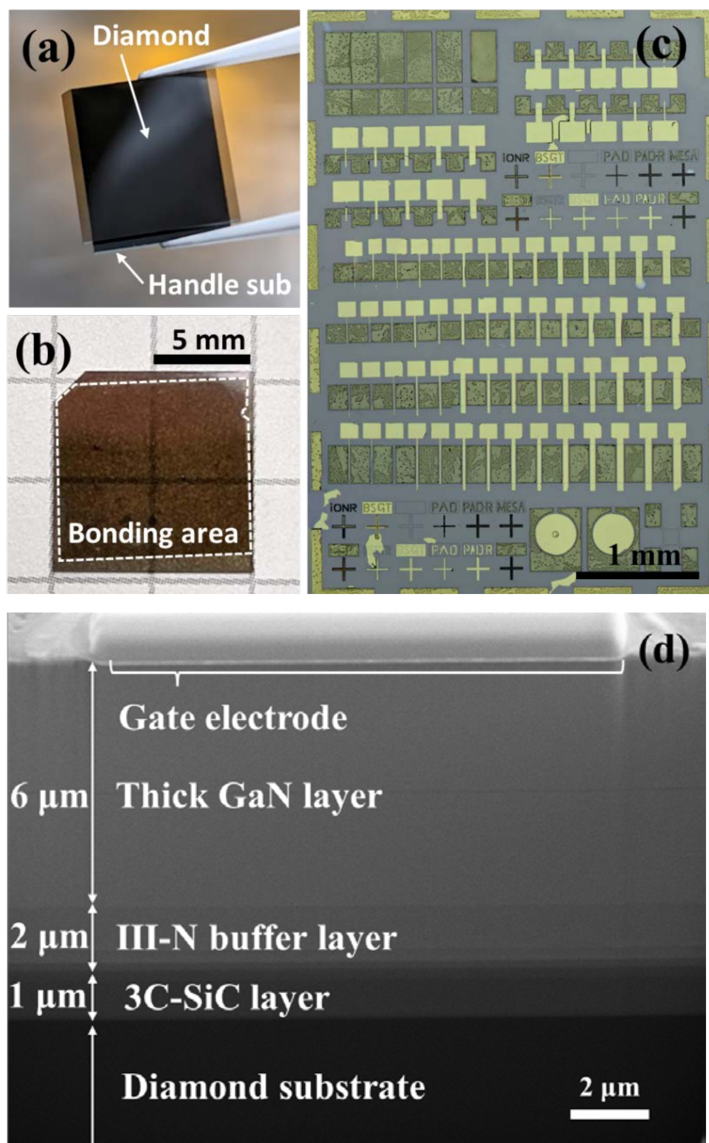

Fig. 2. Top views of (a) as-bonded handle substrate/nitride/3C-SiC/diamond junction, (b) junction after removal of handle substrate, and (c) fabricated on-diamond HEMTs. (d) Cross sectional SEM image of on-diamond HEMTs.

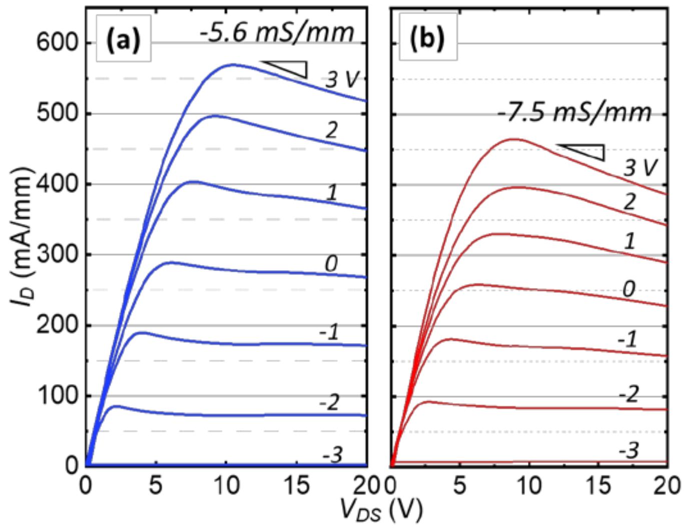

Fig. 3. I_D-V_{DS} characteristics of (a) on-diamond and (b) on-Si HEMTs with L_G = 5 µm, L_{SG} = L_{GD} = 5 µm, and W_G = 150 µm for V_{GS} varied between -4 and 3 V in 1-V steps.

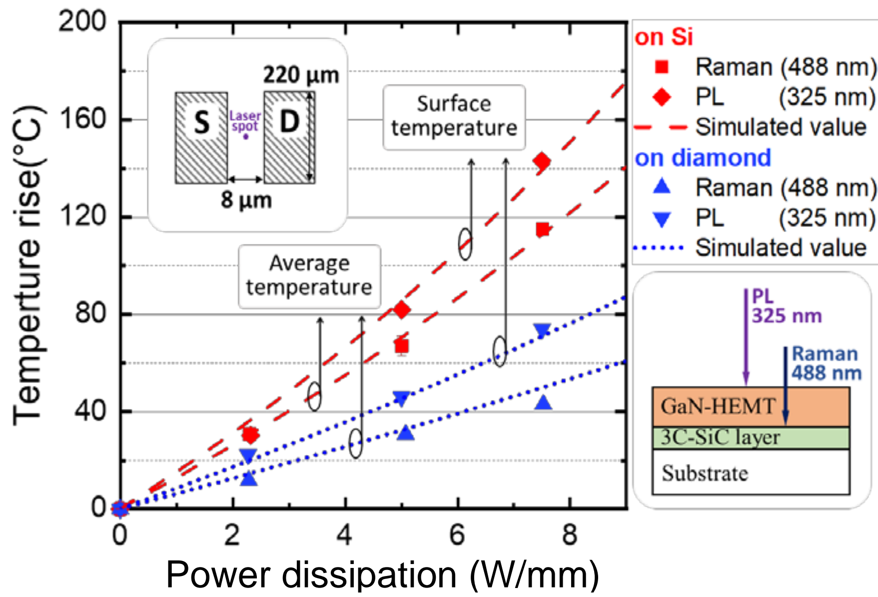

Fig. 4. Relationships between temperature rise and P_{diss} in on-diamond and on-Si TLM devices. Results of measurements based on µ-PL and µ-Raman spectroscopies are compared with those of FEM analysis.

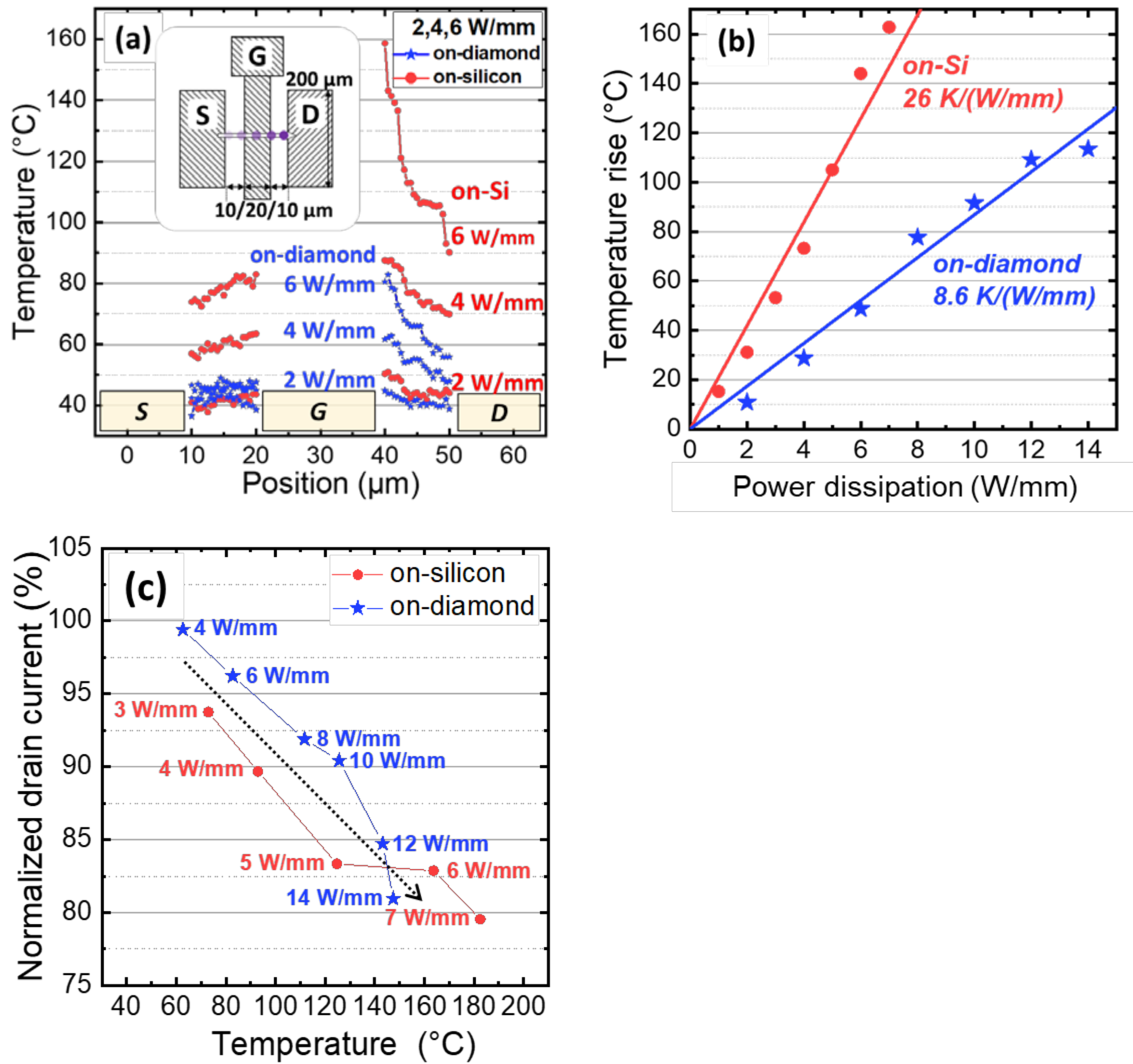

Fig. 5. (a) Spatial variations of temperature on surfaces of on-diamond and on-Si HEMTs for P_{diss} of 2, 4, and 6 W/mm. (b) Relationships between temperature rise at the gate edge in the gate-to-drain separation and P_{diss} for the respective HEMTs. The two lines are eye guides. (c) Relationships between drain current normalized by I_D at P_{diss} of 2 W/mm and the temperature at the gate edge in the gate-to-drain separation for the respective HEMTs.